NANO LETTERS

2008
Vol. 8, No. 8
2570-2575

Micro- and Nanocubes of Carbon with C_8-like and Blue Luminescence

P. Liu, Y. L. Cao, C. X. Wang, X. Y. Chen, and G. W. Yang*

State Key Laboratory of Optoelectronic Materials and Technologies, Institute of Optoelectronic and Functional Composite Materials, School of Physics Science & Engineering, Zhongshan University, Guangzhou 510275, People's Republic of China

Received May 14, 2008; Revised Manuscript Received June 29, 2008

ABSTRACT

Micro- and nanocubes of carbon have been synthesized by laser ablation in liquid. The morphology and structure analyses indicated that these micro- and nanocubes are single crystals with a body-centered cubic structure with a lattice constant of 5.46 Å, which is so-called C_8-like structure, and they have a slightly truncated shape bounded mainly by {200} facets. A blue-purple luminescence at room temperature was observed in the cathodoluminescence spectrum of the synthesized single micro- and nanocube of carbon, which exhibited that this unique carbon nanomaterial is a new semiconductor with blue luminescence. The physical and chemical mechanisms of the synthesis of carbon micro- and nanocubes were pursued upon laser ablation in liquid.

Extensive researches of systematic control and production of inorganic nanomaterials have been devoted for many years because of their size- or shape-dependent properties and the potentials of self-assembly as building blocks for diverse superstructures.[1] In terms of fundamental properties and technological innovations, carbon nanomaterials such as fullerenes, carbon nanotubes, and nanodiamonds have become popular fields for chemists, physicists, and materials scientists.[2,3] Interestingly, nanocubes with wide applications have attracted special interest from both theoretical and applicable perspectives because of their shape-dependent properties,[4,5] and many techniques have been developed to prepare nanocubes.[6−8] However, only metal and metal oxides nanocubes have been intensively studied,[6−10] and there have been few works involved in the semiconductor nanocubes in the present securable literatures.[11−14] Very recently, laser ablation in liquid has become an increasingly important stratagem to synthesize nanostructural materials with metastable phases (structure and shape).[15,16] For instance, laser ablation of a solid target in confining liquid, that is, pulsed-laser induced liquid−solid interface reaction (PLIIR), has been demonstrated to be an effective and general route to synthesize nanostructures, especially for the metastable phase nanocrystals such as diamond and related materials.[16] Here, we show that a kind of novel carbon micro- and nanocubes is, for the first time, synthesized by PLIIR. Interestingly, we find that the synthesized carbon micro- and nanocubes are single crystals with a body-centered cubic (bcc) structure with a lattice constant of 5.46 Å, and it has a so-called C_8-like structure.[17] Importantly, a blue-purple luminescence of the single carbon micro- and nanocube is observed in the cathodoluminescence spectrum at room temperature, which exhibits that this unique carbon nanomaterial is a new semiconductor with blue luminescence. We anticipate our synthesis to be a starting point for more semiconductor micro- and nanocubes fabrications by laser ablation in liquid. Furthermore, the fascinating property of semiconductor micro- and nanocubes is expected to be applicable to fabricate nanodevices as a novel building block.

In the typical PLIIR synthesis,[16] the solid targets are improved to be single silicon substrates covered with 150∼300 nm thick amorphous carbons that are deposited by a filtered cathode vacuum arc (FCVA) technique with the pressure of 3×10^{-5} Torr and the substrate temperature of 300 K. The liquid is selected to be the twice-distilled water mixture of ethanol, acetone, and very low-concentration inorganic salts solutions (≤4 mM) such as KCl (99.5%) and NaCl (99.5%) solutions. A second harmonic is produced by a Q-switched Nd:YAG laser with wavelength of 532 nm, pulse width of 10 ns, a maximum power density of 10^{10} W/cm^2, and the maximum repetition rate of 10 Hz. First, the solid target is fixed on the bottom of a quartz chamber. Then, the liquid is poured slowly into the chamber until the target is covered by 2−3 mm. Finally, the pulsed-laser is focused onto the surface of the solid target. The target and liquid are maintained at room temperature, and the target can rotate and move horizontally at a slow speed. After the pulsed-laser interacted with the target for 15 min, the products that dispersed in the liquid are collected on silicon substrates as the sample in our case. The samples are washed and dialyzed carefully with deionized water for 1 h to remove

* Corresponding author. E-mail: stsygw@mail.sysu.edu.cn.

10.1021/nl801392v CCC: $40.75
Published on Web 07/24/2008

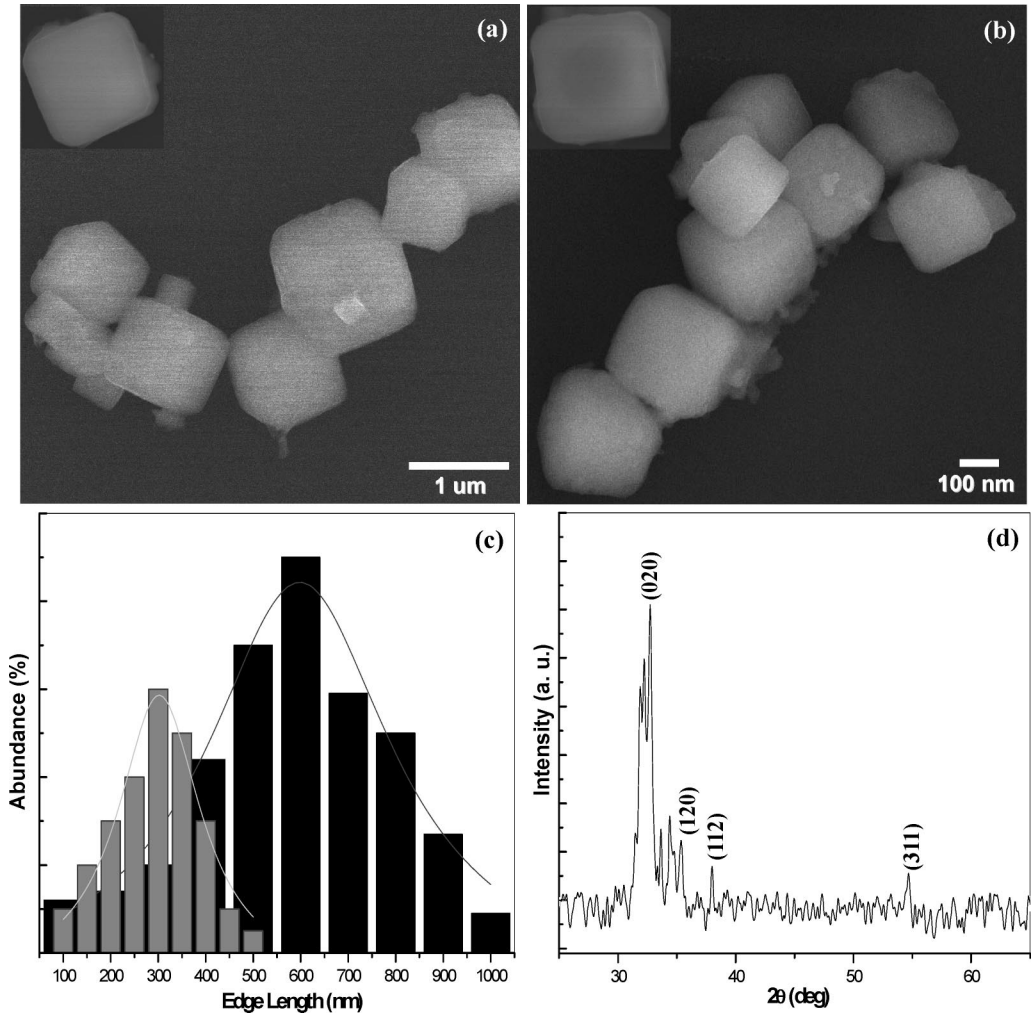

Figure 1. SEM images of the synthesized carbon micro- and nanocubes (a,b), and the insets are high-magnification SEM images of slightly truncated carbon nanocube. Two distribution histograms of the size ration of cubes are shown in c. The corresponding XRD pattern is shown d.

the remaining inorganic salts, and then dried at 40 °C in an oven for several hours before they are measured.

Figure 1 shows two typical scanning electron microscopy (SEM) images of the micro- and nanocubes, and the energy dispersive X-ray spectra (EDS) indicates that these micro- and nanocubes are mainly composed of carbon within the measurement error of 4%. Figure 1a exhibits that these micro- and nanocubes of carbon have perfect three-dimensional geometry, and a high magnification SEM image (the inset of Figure 1a) shows that all corners of micro- and nanocubes are slightly truncated, and the averaged edge length of cubes shown in Figure 1a can be up to about 1 μm. Since the pulsed-laser continuously interacts with the target and then makes not only one but also a large number of times of the quenching process in the initial synthesis, some clusters that mainly locked into the cubic morphology continuously grow up to larger particles. Thus, this results in a broad size distribution of the products. For controllable fabrication, we place the synthesis system in a vibrator with oscillate frequency of 60 kHz to make the size distribution of products become more controlling. Figure 1b shows the improvement. Interestingly, Figure 1b indicates that the synthesized carbon micro- and nanocubes have a relatively narrower size distribution compared with Figure 1a. On the basis of SEM analysis, two distribution histograms of edge length ration of cubes are determined and shown in Figure 1c; that is, the black histogram displays an initial distribution, and the gray chart gives a modified one. Accordingly, these results show that the size of products is relatively controllable in our case. The corresponding X-ray diffraction (XRD) pattern is shown in Figure 1d. Note that no JCPDS data in present literatures can be definitely referred to match our XRD results. According to the systemic analysis of selected area electron diffraction (SAED) data (the next section), four peaks are hypothetically determined to be diffracted from (200), (120), (112), and (311) crystalline planes of a new cubic structure of carbon. Other peaks may be from the SiO_2 layer of Si substrates and other carbon phases.

Figure 2a shows a transmission electron microscopy (TEM) bright-field image of an individual nanocube, which illustrates the high symmetry of a cubic morphology. The corresponding EDS is shown in Figure 2b, which gives an exact identification of the composition of the nanocube within the measurement error of 2%. Thus, the EDS spectrum clearly indicates that the nanocube is almost completely composed of carbon (92%). Additionally, the O (4%) and

Figure 2

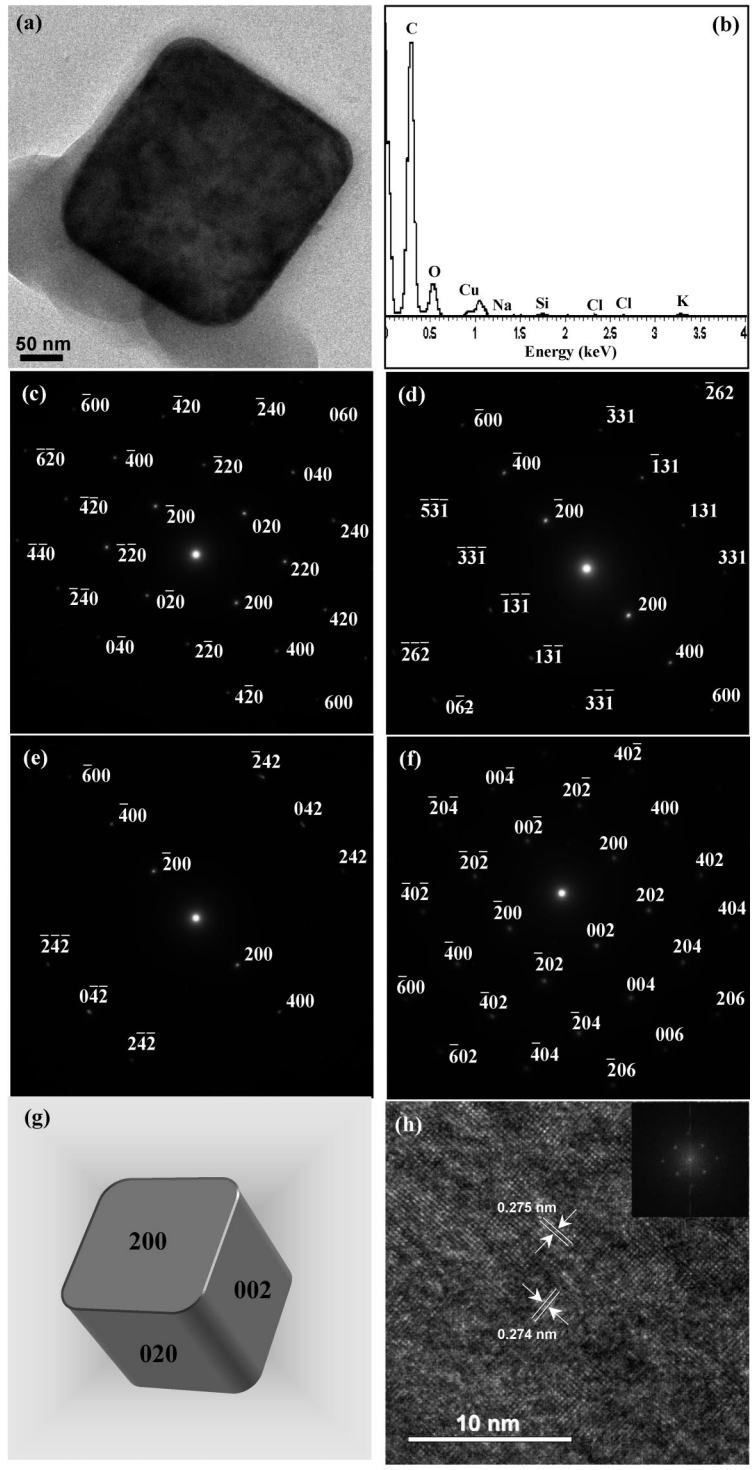

17

Figure 2. TEM bright-field image of a carbon nanocube (a), the corresponding EDS spectrum (b), and the corresponding SAED patterns of one square facet of a carbon nanocube (c). The SAED patterns obtained by directing the electron beam irradiate on different crystal axis of the nanocube (d,e). The pattern of the other square facet of the cube (f). Schematic illustration of the facets of the carbon nanocube (g) and HRTEM image of the (002) facet of the carbon nanocube (h).

Cu (3%) peaks come from the absorbed O_2 molecule on the surface of sample and the copper grid, and the slight Si, Na, K, and Cl weak peaks are supposed to originate from the Si substrate fragments and solution impurity, respectively. For a determination of the crystal structure of these micro- and nanocubes, a great many SAED patterns are analyzed, and in all of these measurement series, the microscope is previously carefully calibrated using the standard inside-gold determination. Figure 2c−f shows a series of the SAED patterns measured by tilting one cube holding on a certain axis. Figure 2c is first recorded by directing the electron beam perpendicular to one of the square faces of the nanocube,

and then the nanocube is rotated, and two SAED patterns (Figure 2d,e) are obtained respectively in this process. At last, the electron beam is directed perpendicular to the other square face of the nanocube, and the SAED pattern of Figure 2f is recorded. On the basis of these consecutive SAED data, we employ a method called reduced-cell-indexing theory to construct a reduced primitive cell matrix.[18] Based on these careful analyses above, the carbon nanocube is identified to have a cubic structure, and the cell parameter is calculated to be about $a = 5.46$ Å. Further, these carbon micro- and nanocubes are suggested to be single crystal bounded mainly by {200} facets, as schematically illustrated in Figure 2g, and the interplanar spacing of (200), (020), and (002) planes are both deduced to be 2.731 Å. For the sake of further confirming the proposed results, a high-resolution TEM (HRTEM) image of one facet of a nanocube is recorded and shown in Figure 2h. The dominant two-dimensional lattice fringes exhibited in Figure 2h is measured to be 0.275 and 0.274 nm, respectively. Additionally, a corresponding fast Fourier transform (FFT) analysis (inset in Figure 2h) indicates that the two kinds of lattice fringe directions are (200) and (020), respectively. Considering the error in the lattice parameter determined by HRTEM, these two interplanar spacings are thus in agreement with our calculations above. Accordingly, on the basis of TEM, SAED, and HRTEM analyses, we conclude that carbon micro- and nanocubes with a new cubic structure are synthesized for the first time by laser ablation in liquid.

To clarify the discovery of the unique cubic structure by theoretical method, a full-potential linear augmented plane wave plus local orbital (FP-LAPW+LO) with density-functional theory, which is implemented in the software WIEN2K,[19] is employed to calculate the cubic lattice structure and the corresponding convergence state of total energy of the carbon micro- and nanocubes. The new cubic phase is suggested to be a new bcc structure, that is, the so-called C_8-like structure. Figure 3a exhibits a crystal framework sketch map of the imagined C_8-like structure, and Figure 3b exhibits the corresponding total energies per cell. Definitely, we can see that the C_8-like structure is stable and converges to the lowest energy when the cell parameter is about 5.432 Å, which is well-consistent with the experimental date (5.46 Å) from the TEM analysis. Therefore, these calculations above confirm the conclusion from the experiment.

Figure 4a shows an SEM image of four nanocubes on a silicon substrate, and the corresponding cathodoluminescence (CL) image and the CL spectrum at room temperature are shown in the inset of Figure 4a and in Figure 4b, respectively. Surprisingly, a clearly blue-purple luminescence with a broad emission band from 366 to 450 nm is observed in the CL spectrum, in which three small peaks at 366, 393, and 412 nm can be distinguished in the broadband. Therefore, these findings indicate that the carbon micro- and nanocube is a new semiconductor with blue luminescence. Figure 4c,d shows a photoluminescence (PL) spectrum of the as-synthesized sample and a corresponding ultraviolet absorption (UV) spectrum. Clearly, we can see that there is a broad

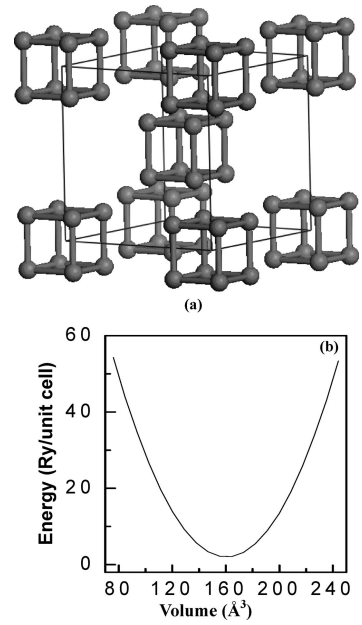

Figure 3. Crystal structure of a C_8-like configuration with the cubic *IM*-3 spacegroup (a). Corresponded calculated total energies shows a function of primitive cell volume of the C_8-like structure (b).

luminescence peak appears around 360 to 450 nm in the PL spectrum, and three effective peaks at 367, 393, and 432 nm can be distinguished in the broadband. The positions of these three PL peaks are basically the same to that of CL shown in Figure 4b. Thus, these results again indicate that the carbon micro- and nanocube are a kind of wide band gap semiconductor with blue luminescence. Considering the wavelength of the excitated light of 230 nm is used in our measurement, the small luminescence peak at 462 nm is suggested to originate from the twice luminescence caused by the excited light, which is not eliminated completely by the filtration glass.

Figure 4d shows a UV absorption spectrum of carbon micro- and cubes, in which there are three broad absorption peaks marked by A, B, and C, respectively. On the basis of the PL analyses above, the broad peak at A is supposed to be the intrinsic absorption peak of the micro- and nanocubes. Essentially, the optical properties of materials are determined by the energy band. Then, the shape and size of nanoparticles may have great influence on their optical properties by affecting the status of polarization (extrinsic) as well as adjusting the energy band structure (intrinsic).[20] Thus, the peaks at B and C are suggested to be an absorption cross section that is influenced by the distribution of dipole or electric field of sample, which could be caused by the shape or size of the micro- and nanocubes. For further studying the band gap structure of these microand nanocubes, we calculate the band structure of the carbon microand nanocubes by first-principle method on the basis of the experimental data above (Figure 3a), and the calculations are shown in Figure 4e. Interestingly, Figure 4e indicates that the micro- and nanocubes of carbon have an indirect band gap. Thus, the experimental luminescence peaks are supposedly from the surface states, which induce the surface trap bands among the indirect band gap. An illustration in Figure 4e shows

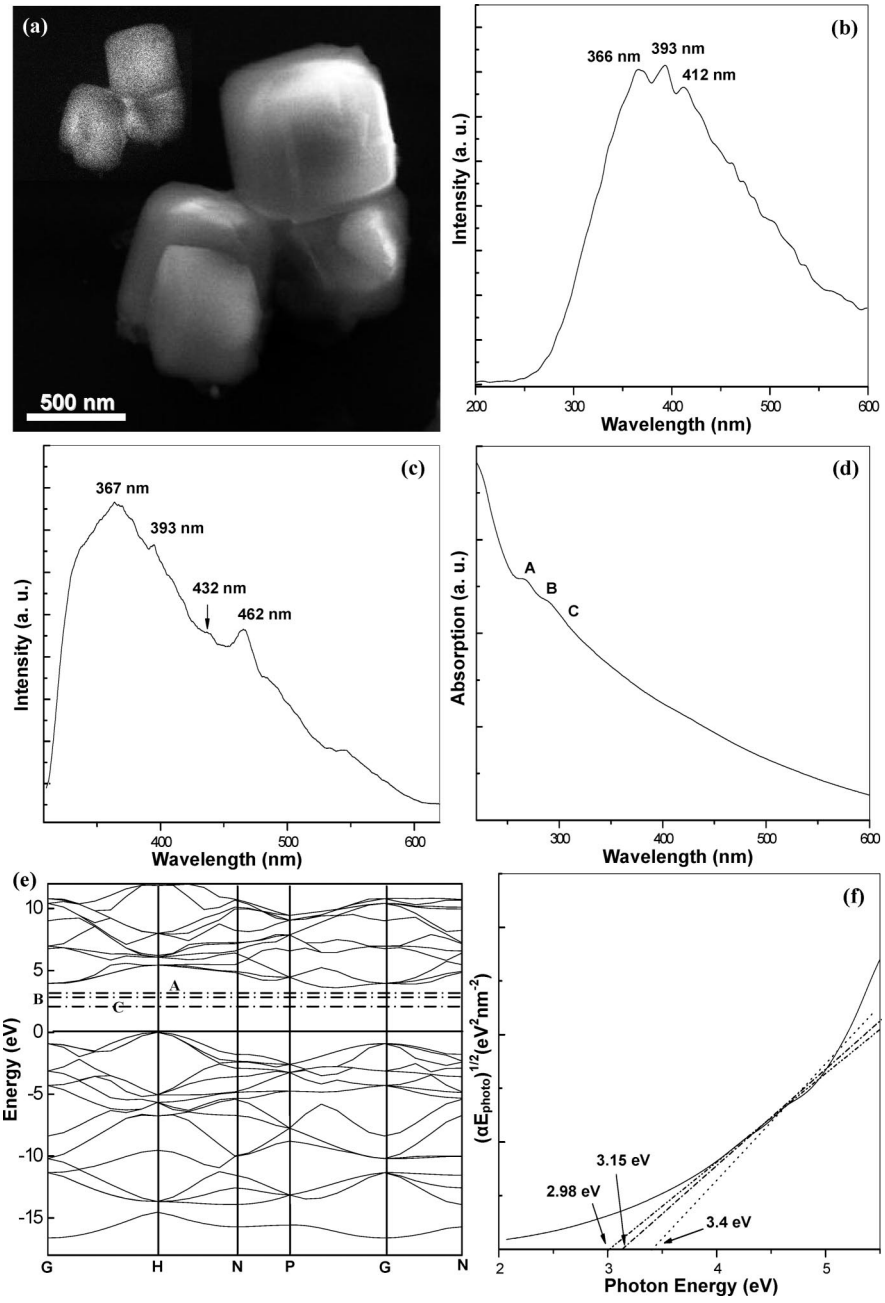

Figure 4. SEM image of four single carbon nanocubes, in which the inset shows the corresponding CL image (a), and the corresponding CL spectrum (b). A PL spectrum and a UV absorption spectrum are shown in c,d. The calculated energy band structure of the carbon nanocube is shown in e, in which the band gap is modified mainly by the CL analysis. Part f exhibits an energy intercept of plots of $(\alpha h\nu)^{1/2}$ vs E_{photo}, which indicates three deduced band gaps in this analysis.

three dot lines of the surface trap bands with the energy gaps of 3.38, 3.15, and 2.86 eV, respectively. Moreover, Figure 4f shows the $(\alpha h\nu)^{1/2}$ versus E_{photo} curve which yields E_g for the sample based on the equation[21] $(\alpha h\nu)^n = B(h\nu - E_g)$ with the data gained from the UV absorption analysis, and three band gaps of the as-synthesized micro- and nanocubes are thus deduced to be about 3.35, 3.15, and 2.98 eV from the extrapolation of the linear section of the graph to $(\alpha h\nu)^{1/2} = 0$, which are apparently in agreement with our theoretical band gap above.

Compared with cubic and hexagonal diamond, the new bcc structural carbon with lattice constant of 5.46 Å in our case (Figure 3a) has remarkable characters as follows. Structurally, there are 8 carbon atoms in the primitive lattice and 16 equivalent carbon atoms in the C_8-like structure that forms a distorted cubic environment, which creates a bcc phase and is clearly different from the fcc or hexagonal phase of the diamond structure. Moreover, the configuration indicates that the distorted C−C bonds are present in the C_8-like structure and these bonds are unlike the normal C−C single bond that exists in the diamond structure and induces a distorted sp^3 bonding in the C_8-like structure. In the structural energy band, we can see that the C_8-like structure has a wide but indirect band gap based on the first-principles calculations (Figure 4e). Since the clear luminescence is observed from the CL spectrum and the PL characterization,

we suggest that the luminescence should be caused by surface states. These surface states induce the surface trap bands among the indirect band gap and finally cause the blue-purple luminescence of the micro- and nanocubes of carbon.

Generally, PLIIR is a very fast and far from equilibrium process, so that all stable and metastable phases forming at the initial, intermediate, and final stage of laser ablation in liquid could be reserved in the final products.[16] The initial process of laser ablation at the liquid−solid interface is an interaction between laser and solid target. The species having a large initial kinetic energy first form a dense region in the vicinity of the solid−liquid interface, called the laser-induced plasma plume. Then, a shock wave will be created at supersonic velocity in front, which will induce an extra pressure in the plasma plume, called the laser-induced pressure, due to the liquid confinement. Thus, the laser-induced pressure induces a temperature increase in the plasma plume. Finally, the plasma plume from laser ablation in liquid is in the high-temperature, high-density, and high-pressures (HTHDHP) state. As another result of the liquid confinement, the quenching time of the plasma plume become so short that the metastable phase could be frozen in the final products.[22] Additionally, because the growth time (the plasma quenching time) of the nuclei is very short, the size of the grown crystals is usually in the nanometer scale.[23] For our case, the laser-induced plasma including many kinds of carbon species is first generated at the liquid−solid interface when pulsed-laser ablating the amorphous carbons. The incident laser irradiation drives the plasma plume into a HTHPHD state, in which the chemical reactions and the phase transitions would happen. Sequentially, a rapid quenching of the plasma plume will lead to the nucleation of the forming phases and the growth of the nuclei. Note that the inorganic salt ions existing in the liquid play an important role in the nucleation and growth of crystals.[24] Since the inorganic salts used in our case belong to the cubic structure crystal, they always tend to nucleate as a cube. Therefore, the inorganic salt ions inner and around the plume will act as a template to induce the nucleation and growth of the carbon in the quenching process. In detail, these salt ions adsorb onto a certain crystallographic plane more strongly than others because of the anisotropy in adsorption stability. Accordingly, this preferential adsorption lowers the surface energy of the bound plane, hinders the crystal growth perpendicular to this plane, and results in a change in the final morphology.[25] Therefore, the final products are locked into a cubic morphology in single crystalline by the salt−ion−template effect.

In summary, the carbon micro- and nanocubes with a new bcc structure have been, for the first time, synthesized by pulsed-laser induced liquid−solid interface reaction in low-concentration inorganic salts solutions. A blue-purple luminescence in the CL spectrum of single carbon micro- and nanocubes indicates that this novel carbon nanomaterial is a new wide band gap semiconductor.

Acknowledgment. This work is supported by the National Natural Science Foundation of China (50525206, 10474140, and U0734004) and the Ministry of Education (106126).

References

(1) Li, F.; Qiang, F.; Xiang, J.; Lieber, C. M. *Mater. Today* **2006**, *9*, 18.
(2) Pichler, T. *Nat. Mater.* **2007**, *6*, 332.
(3) Geim, A. K.; Novoselov, K. S. *Nat. Mater.* **2007**, *6*, 183.
(4)
(5) Murphy, C. J. *Science* **2002**, *298*, 2139.
(6) Chan, E. R.; Zhang, X.; Lee, C. Y.; Neurock, M.; Glotzer, S. C. *Macromolecules* **2005**, *38*, 6168.
(7) Liu, R.; Oba, F.; Bohannan, E. W.; Ernst, F.; Switzer, J. A. *Chem. Mater.* **2003**, *15*, 4882.
(8) Xu, R.; Zeng, H. C. *Langmuir* **2004**, *20*, 9780.
(9) Dumestre, F.; Chaudret, B.; Amiens, C.; Renaud, P.; Fejes, P. *Science* **2004**, *303*, 821.
(10) Sun, Y.; Xia, X. *Science* **2002**, *298*, 2176.
(11) Gou, L.; Murphy, C. J. *Nano Lett.* **2003**, *3*, 231.
(12) Kanemitsu, Y. *Phys. Rev. B* **1995**, *51*, 10666.
(13) Motiei, M.; Calderon-Moreno, J.; Gedanken, A. *Adv. Mater.* **2002**, *14*, 1169.
(14) Wang, W.; Huang, J.; Ren, Z. *Langmuir* **2005**, *21*, 751.
(15) Citroni, M.; Ceppatelli, M.; Bini, R.; Schettino, V. *Science* **2002**, *295*, 2058.
(16) Yang, G. W. *Prog. Mater. Sci.* **2007**, *52*, 648.
(17) Johnston, R. L.; Hoffmann, R. *J. Am. Chem. Soc.* **1989**, *111*, 810.
(18) (a) Guo, K. K. *Acta Physica Sinica* **1978**, *27*, 160. (b) , *Acta Physica Sinica* **1978**, *27*, 473.
(19) Perdew, J. P.; Burke, K.; Ernzerhof, M. *Phy. Rev. Lett.* **1996**, *77*, 3865.
(20) Chen, X. Y.; Cui, H.; Liu, P.; Yang, G. W. *Appl. Phys. Lett.* **2007**, *90*, 183118.
(21) Tauc, J.; Grigorovici, R.; Vancu, A. *Phys. Status Solidi* **1966**, *15*, 627.
(22) Yang, G. W.; Wang, J. B. *Appl. Phys. A: Mater. Sci. Process.* **2001**, *72*, 475.
(23) Wang, C. X.; Liu, P.; Cui, H.; Yang, G. W. *Appl. Phys. Lett.* **2005**, *87*, 201913.
(24) Wiley, B.; Herricks, T.; Sun, Y.; Xia, Y. *Nano Lett.* **2004**, *4*, 1733.
(25) Yang, S. W.; Gao, L. *J. Am. Chem. Soc.* **2006**, *128*, 9330.

NL801392V